Thermographic study of heat load asymmetries during MAST L-mode discharges

G. De Temmerman[1,2], E. Delchambre[3], A. Kirk[2], S. Lisgo[4], and P. Tamain[2]

[1]Present address: FOM Institute for Plasma Physics Rijnhuizen, Edisonbaan 14, 3439 MN Nieuwegein, The Netherlands

[2]EURATOM/UKAEA Fusion Association, Culham Science Centre, Abingdon, UK

[3]Association Euratom-CEA, CEA/DSM/IRFM, CEA Cadarache, F-13108 Saint-Paul-ls-Durance cedex, France

[4]ITER Organization, CEA-Cadarache Centre, 13108 Saint Paul les Durance, France

E-mail: g.c.temmerman@rijnhuizen.nl

Abstract.

A long wavelength range infrared camera (LWIR) has been installed on MAST to compliment the existing medium wave infrared system. Simultaneous LWIR/MWIR temperature measurements have been made in the lower and upper divertors of MAST. As expected, the LWIR system is less sensitive to disturbances from hot spots on the surface. A thorough correction of the surface effects using both systems has improved the reliability of the heat flux calculations in MAST. A careful assessment of the heat load asymmetries as a function of the magnetic geometry has been carried out during a variety of L-mode discharges (single and double null, reversed and forward field). In all cases, most of the energy arriving in the SOL goes to the outer divertor. The in/out power ratio is found to be different for lower and upper single null discharges with more power going to the outer divertor in the latter case. In addition, it is found that the heat flux profile width is different in the upper and lower divertor. The heat flux profile width at the secondary strike point increases with increasing δr_{sep}.

PACS numbers: 52.40.Hf, 52.77.Dq

1. Introduction

Plasma-facing components in a fusion reactor will have to be able to handle the high-energy flux which passes through the plasma boundary both during steady-state operations and also during transient events like disruptions and edge localized modes (ELMs) [1]. In order to give designers confidence in planning future devices like ITER, it is important to know the global power balance i.e. the division of power between radiation and conduction/convection losses, and the spatial distribution of heat deposition inside the machine. In addition, the spatial profile of heat deposition on a given surface, characterized by the exponential decay length in the scrape-off layer (SOL) λ_q, is an important parameter as it defines the maximum heat flux the surface will experience.

Power balance studies have been conducted in a number of devices like DIII-D [2], JET [3], ASDEX-Upgrade [4], JFT-2M [5] and MAST [6] where between 80% and 100% of the input power could be accounted for during L-mode discharges. Scalings for the dependence of the heat flux profile width with key discharge parameters have been developed but the scatter in the dependence on the power to the divertor, for example, from the various studies is large and makes extrapolations difficult [7, 8].

Heat fluxes to the surfaces in tokamaks are usually derived using data from infra-red (IR) cameras, langmuir probe arrays or thermocouples. IR cameras allow surface temperature measurements with good spatial and temporal resolutions. Heat fluxes to the surface are derived from the temporal evolution of the surface temperature by solving the heat diffusion equation. The intense plasma-material interactions occuring in a fusion device however strongly modify the surface of the exposed material leading to the appearance of hot spots on the surface [9], or co-deposited layers with thermal properties different from those of the bulk material [11, 12] which can lead to an over-estimation of

the surface temperature and consequently of the calculated heat fluxes. Most tokamaks currently use IR cameras sensitive in the wavelength range 1-5μm (medium wave infrared or MWIR), and it has been shown in [9] that the use of a camera working in the long wave infrared (LWIR, 8-12μm) might help mitigating the hot spot effect for machines which have low temperature carbon plasma-facing components, like MAST. A LWIR camera has been installed on MAST, allowing the verification of this hypothesis and allowing the study of heat load asymmetries in a large variety of plasma configurations.

In this paper we report on the comparison of the temperature measurements in MAST in the LWIR and MWIR ranges and the consequences for heat flux calculations. Cross-calibration of the IR system has allowed a study of the heat load asymmetries during a variety of L-mode discharges with a focus on the influence of the magnetic geometry on the asymmetries and heat flux profile width.

2. Experimental

2.1. MAST IR system

MAST is equipped with 2 infrared cameras. The MWIR camera is a Santa Barbara Focal Plane system (SBFB 125, 320x256 pixels) which measures IR radiation in the wavelength range of 3 to 5 μm. The camera is equipped with a bandpass filter to limit the working wavelength range to the range 4.5-5μm. The maximum framerate of the camera is 10 kHz for a 128x8 pixels sub-window and 315 Hz for full-frame data acquisition. The typical spatial resolution of the system equipped with a standard 15 mm lens is about 5 mm.

Recently a LWIR camera has been installed on MAST. The device itself is a Thermosensorik CMT256 L HS camera with a 256x256 pixel focal plane array detector sensitive in the 7.6-8.9μm wavelength range. The camera acquisition frequency is in the

range 880Hz (full-frame) to 25kHz (sub-array mode). The typical spatial resolution of the LWIR system with a standard 15 mm lens is about 7 mm.

The relative open vessel design of MAST [13] as well as the large vacuum to plasma volume ratio makes MAST exceptionally suited for optical diagnostics. No periscope or re-entrant ports need to be used, and the IR cameras are simply equipped with a commercial lens and installed behind a suitable window (Cleartran and sapphire for the LWIR and MWIR respectively). By installing the cameras at different locations and using lenses with different focal lengths, the camera view and resolution can be adapted. Two views are standardly used and are illustrated in figure 1. Tangential viewing of the outer divertor (figure 1a and b) is typically used for simultaneous MWIR/LWIR temperature measurements and stereoscopic imaging of dust motion (the latter will be described in a separate publication). The cameras can be installed on the same port (slightly shifted toroidally) on either divertor so that they can observe the same region simultaneously. In addition, a second type of geometry is used to observe simultaneously the inner and outer divertors (figure 1c and d), the red box in the figure illustrates the view obtained when working with a sub-array of the detector, in this case the maximum framerate is 6kHz for the MWIR camera and 14.5kHz for the LWIR camera. In this case also, either camera can be installed on either divertor.

The cameras are calibrated in the laboratory using a blackbody source up to 800C. One of the divertor tiles is equipped with a Mica heater and can be heated up to 150C. The internal tile is used to calibrate the cameras in-situ so that the product of the window transmission and tile emissivity can be determined. This procedure is repeated regularly during the campaign to check and correct possible drifts due to modification of the surface emissivity and window transmission.

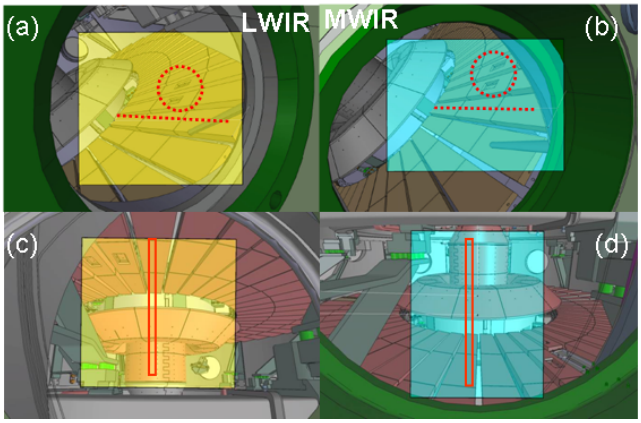

Figure 1. Illustration of the different views that can be obtained from the different possible configurations of the IR cameras in MAST. The 2 left pictures refer to the LWIR camera while the pictures on the right hand side refer to the MWIR camera. Note that the same views are available for both the upper and the lower divertor and for both cameras.

3. Influence of the surface effect at different wavelengths

3.1. Comparison of LWIR and MWIR temperature measurements

The cameras were set-up for simultaneous observations of the same area of either the lower or the upper divertor during a variety of discharges (H-mode, L-mode). The cameras were synchronized in time (using the same clock signal) and had the same framerate. The shots were divided in 20ms segments, and the maximum and minimum temperatures during that segment have been extracted. In addition, data obtained when saturation of one of the camera occured have been rejected. The temperatures determined by both cameras are quite different and the difference depends on the divertor observed (figure 2). For the lower divertor, the LWIR temperatures are 56% lower than the MWIR temperatures while the discrepancy is much lower for the upper divertor (LWIR temperatures are 91% of the MWIR temperatures).

A similar trend i.e. a discrepancy between temperature measurements at different wavelengths was already reported in several studies (see for example [10]). Several effects can lead to an overestimation of the surface temperature. These effects are linked to

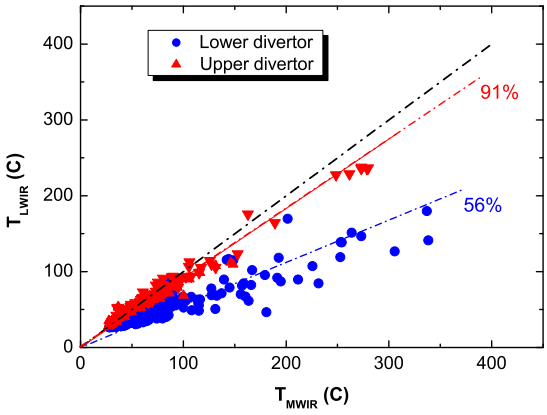

Figure 2. Comparison of the temperatures determined by the MWIR and LWIR cameras during observations of the same area of the lower and upper divertor respectively.

plasma-material interactions, presence of a thick co-deposited layer, as was observed in Tore-Supra [16] and JET [11], or dust particles [14, 9] on the surface with bad thermal contacts with the material bulk , and also to the limited spatial resolution of the IR systems used in most tokamaks compared with the typical dimensions of the material roughness/morphology [17, 18]. Indeed, IR temperature measurements with high spatial resolution (in the micron range) on fine grain graphite and CFC have shown the presence of hot spots on the surface with typical sizes in the range of 30 μm in the case of CFC [15]. Similar effects have been observed for fine grain graphite covered with dust [9], while polished graphite shows a uniform temperature distribution across the surface [9].

In the case of MAST, fine grain graphite is used as the plasma-facing material for the divertor and the centre column. The relatively short pulse duration ($\sim$ 0.5s) and natural sweeping of the strike-points imply that thick co-deposited layers are unlikely to form over a campaign, which has been verified by post-mortem analyses of the divertor tiles [19]. In addition, laboratory experiments using a flash lamp for transient heating of MAST divertor tiles with different preparation techniques have shown that

the presence of dust on the surface was the main disturbance to IR measurements in MAST [9]. Since the emissivity of graphite dust is inversely proportional to the square of the wavelength in the range 1-15μm [20], and that according to Planck's law a high temperature body (like dust in radiative equilibrium on the surface) radiates more in the near-infrared, temperature measurements in the LWIR range should be less disturbed by the presence of dust on the surface. The MAST results (figure 2) confirm this hypothesis. Furthermore, the difference between the LWIR and MWIR temperatures observed for the lower divertor can be reproduced by assuming a certain dust size and surface coverage [21]. In MAST, the $\bigtriangledown B$ drift points towards the lower divertor and more power is expected to flow towards the lower divertor in DND discharges, thus the surface temperature is expected to be lower in the upper divertor than in the lower divertor which constrasts with the experimental observations (figure 2). In addition, the lower discrepancy observed for the temperature measurements on the upper divertor would imply a lower dust coverage of these surfaces, which is consistent with observations of dust particles released from the upper divertor during a disruption and falling downwards. This will be described in more details in the next session.

3.2. Heat flux calculations

The target heat fluxes in MAST are calculated using THEODOR [23], a 2D inverse heat transfer code which considers the presence of a layer on top of the substrate. The layer is characterized with a given α parameter, the ratio of the heat conductivity to the thickness of the layer [22]. Without this parameter, negative heat fluxes can be calculated by the code because of the over-estimation of the surface temperature induced by the bad thermal contact of the disturbed layer with the bulk. It has been shown previously that this concept also holds in the case of hot spots on the surface [24]. In order to determine the values of alpha to be used for both cameras and both divertors,

the method described in [24] and [25] is used, i.e. the value of α is varied until negative heat fluxes are removed. This work has been done independently on both cameras. Results obtained for L-mode double null discharges are shown in figure 3. Due to the constant strike point sweeping in MAST, negative heat fluxes are usually apparent on the heat flux profile before the strike point. In order to suppress this negative value at the lower divertor a value of α_{MWIR}^{lower}=70 $kW \cdot m^{-2} \cdot K^{-1}$ is needed for the MWIR, while a higher value of α_{LWIR}^{lower}=300 $kW \cdot m^{-2} \cdot K^{-1}$ is needed for the LWIR camera. It should be precised that the higher α the lower the correction for the surface layer. A similar trend is observed for the upper divertor, although both values of α are lower. With such values the heat flux profiles from both cameras are in pretty good agreement for the heat fluxes considered here. In addition, different values of α are used for the outer and inner divertors, and different values are also needed during ELMs (not considered here) [24].

It is also striking that when looking at the evolution of the total deposited energy (integrated toroidally and over a shot) as a function of α, the optimum value of alpha for both cameras sits at different location on the obtained curve (fig. 3 c and d). For the lower divertor (fig. 3c), the optimum value of α (i.e. the first value allowing a suppression of the negative heat fluxes) for the lower divertor sits at the knee of the curve while in the MWIR case, it sits in the steepest part of the curve. On the other hand, for the upper divertor, the optimum point for both cameras sits in the steepest part of the curve.

The lower α values needed for the LWIR camera are in agreement with the systematic overestimation of the temperature by the MWIR camera in fig. 2. In addition the difference between α_{LWIR} and α_{MWIR} is the highest for the lower divertor while both values are much closer for the upper divertor, this is also in agreement with the lower

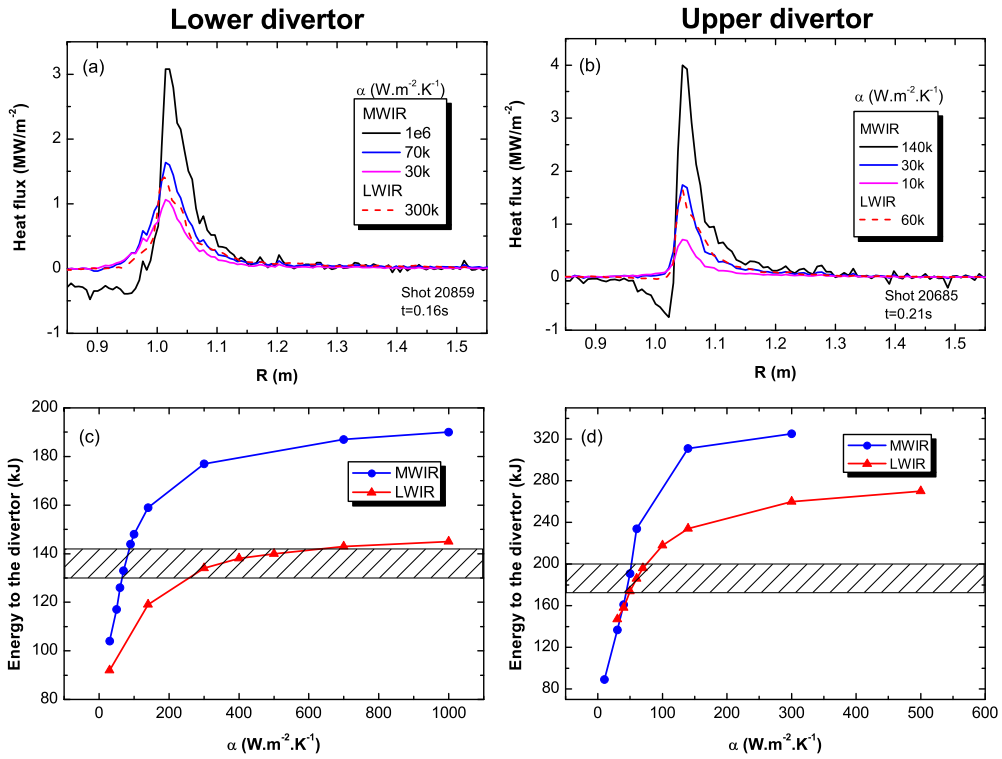

Figure 3. Evolution of the heat flux profile as a function of the α value used in THEODOR for the lower (a) and upper (b) divertors. For clarity, for the LWIR camera, only the profile with the optimized value of α is shown. (c) and (d) show the evolution of the total energy over a discharge vs. α for the lower and upper divertor respectively. The shaded area shows the probable energy band from EFIT, taking into account the uncertainties in the power repartition between the 2 divertors.

temperature differences measured for the upper divertor although α^{upper} is higher than α^{lower}. It therefore appears that the surface effect is more prominent for the upper divertor (i.e. lower α required). As mentioned earlier, dust is observed to fall down from the upper divertor after each disruption, and motion of dust particles is regularly observed in the outer divertor. Micrometer-size dust particles have been collected on the lower divertor during a machine opening [26]. In DND operations, the electron temperature is usually higher in the lower divertor than in the upper divertor, so that if one makes the analogy between the upper divertor of MAST and the inner divertor of

tokamak like JET, one might expect that similarly to what is observed on JET where the inner divertor is a zone of net deposition [27], the upper divertor in MAST might be an area of net deposition while the lower divertor would be a zone of net erosion or balance between net erosion and deposition. In such a case, temperature measurements on the upper divertor might be hampered by co-deposited layers while dust would disturb the measurements on the lower divertor. Post mortem analyses of tiles from those 2 regions would be needed to check this hypothesis.

Fig. 4 a, shows a comparison of the integrated energy at the outer divertor determined for L-mode discharges where both cameras were observing the same region. A relatively good agreement is obtained through a wide range of energy which confirms the appropriate choice of α as described previously. In addition, since this study aimed at studying the evolution of the heat flux profile width, the values obtained for both cameras (averaged on segments of 20ms) have been compared (fig. 4b) and are found to be in good agreement, although the LWIR camera seems to derive values which are slightly higher than the MWIR values. This might be due to the poorer spatial resolution of the LWIR system. In addition, the integration time of the LWIR camera is systematically lower than that of the MWIR camera for similar temperature ranges, the LWIR camera might then be more sensitive to fluctuations around the strike-point whilst and indeed filamentary structures are more clearly observed on the LWIR camera (more details in the next sessions).

4. Heat load asymmetries

4.1. Power balance

The study of head load asymmetries in MAST was performed with the cameras installed in the views (c) and (d) of fig. 1. For a varietey of different plasma configurations (SND,

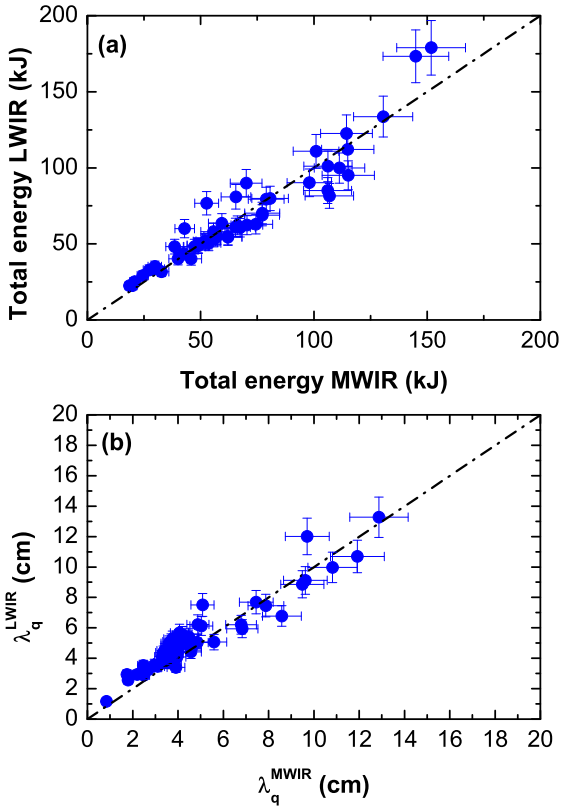

Figure 4. (a) Comparison of the total integrated energy and (b) heat flux profile width, determined from both cameras when observing the same area.

DND, forward and reversed field), the energy flowing to the divertor (integrated over the 4 strike points) has been compared to the energy arriving into the SOL. The latter is defined as the sum of the ohmic and auxilliary power input to the core plasma less the rate of change of stored energy and radiated power (as determined from bolometry measurements). In comparison to what was observed in DIII-D [2] where significant amounts (5-20%) of energy reaches the first wall, no such interaction occurs in MAST due to the large distance between the edge plasma and the outer wall. As evident from fig. 5, during L-mode discharges, around 100% of the SOL energy arrives at the divertor target, so that the IR cameras provide a very good power accounting. The same trend is observed for DND and SND discharges as well as during DND discharges with reversed

magnetic field. This is in good agreement with previous studies on MAST using target langmuir probes [6].

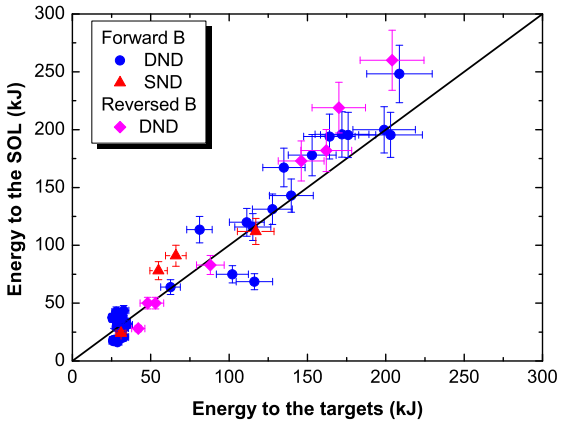

Figure 5. Total energy arriving at the target from IR thermography versus energy arriving in the SOL for different plasma configurations.

4.2. Heat load asymmetries

The effect of the magnetic configuration on the up/down and in/out heat load asymmetries has been studied by shifting an ohmic discharge (I_p=600kA, $\bar{n}_e$=7-8×10^{19}m^{-2}) up and down progressively. The same discharge was repeated with different reference vertical position of the plasma axis. This way the distance between the 2 separatrices at the outer midplane (δr_{sep}) was varied between -4.5 and 4.5 cm (negative values refer to lower single null discharges) keeping the plasma parameters fixed. The results are shown in figure 6. In addition, data from a collection of MAST-L mode discharges have been added. It should be noted however, that the standard operating mode of MAST consists of DND discharges with only slight variations of δr_{sep} which is known to affect the H-mode access. Finally, data obtained during a campaign of reversed magnetic field operations are added to the graph.

The curve obtained for the up-down power distribution as a function of δr_{sep} (fig.

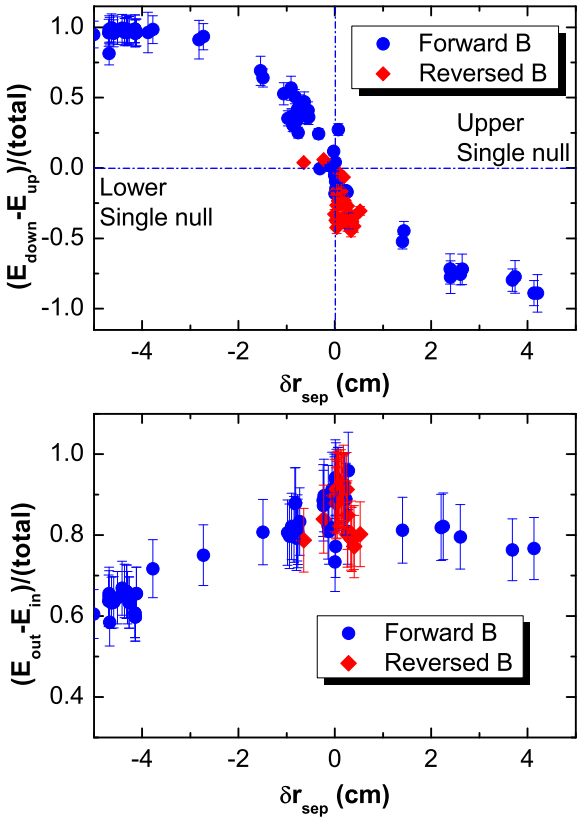

Figure 6. Energy distribution during MAST L-mode discharges. Difference between (a) energy to lower and upper divertors and (b) between energy to outer and inner divertors versus the distance between the 2 separatrices at the midplane.

6a) is similar to that obtained in DIII-D [2]. For a magnetically balanced case and forward magnetic field, more power generally goes to the lower divertor towards which points the $\bigtriangledown B$ drift direction. Up-down symmetry was previously found to occur for a δr_{sep} value of about 2 mm [6]. The same behaviour is observed in the reversed field case i.e. that the power goes preferentially to the upper divertor when the $\bigtriangledown B$ drift is directed towards it, it should be mentioned that the range of δr_{sep} values for that case is relatively limited. The transition between all power flowing to the lower divertor and all flowing to the upper divertor is relatively smooth.

The evolution of the in-out power distribution as a function of δr_{sep} (fig. 6b) reveals

interesting features. As already observed [6], in DND discharges, most of the energy leaving the core plasma flows to the outer divertor. The observed ratio of power arriving at the outer strike-points to that at the inboard strike points lies in the range 20-40 and is strongly peaked for δr_{sep} close to 0. It has been observed in machines like ASDEX and PDX where the observed asymmetry was close to the ratio of the outer and inner SOL surface areas combined with the ratio of flux compression [28]. The situation is quite different in MAST where the ratio of the surface areas of the separatrices is around 4 and the ratio of flux compressions is around 3, which might imply that a different transport mechanism is at stake. The in-out power distribution is different for lower and upper single null discharges with comparatively more energy flowing to the outer divertor in the latter case. It is worth noting that such an asymmetric behaviour was not reported in [6] but in that case δr_{sep} was only varied in the range -1.5 to 1.5 cm. For a similar range in fig. 6, a similar conclusion would be drawn. When extending the range however, it is clear that a different behaviour is observed. Actually, the evolution of the in-out power asymmetry seems to flatten out for δr_{sep} higher than 2cm, while there is a continuous change for negative δr_{sep} with more and more power going to the inner divertor.

4.3. Evolution of the heat flux profile

The evolution of the heat flux profile width at the outboard or low field side (LFS), λ_q, with the distance between both separatrices is shown in figure 7a, where values obtained for the upper and lower divertors are shown even when the plasma is in single null configuration to illustrate what happens at the secondary strike point. The large scatter of λ_q around the magnetically balanced configuration can be explained by the dependence of λ_q on the plasma density, magnetic field, safety factor and power crossing the separatrix [8]. When the plasma is moved away from the magnetically balanced

situation, the evolution of the heat flux profile width with δr_{sep} depends on the sign of δr_{sep} (fig. 7a). When the $\bigtriangledown B$ drift direction points towards the lower divertor, λ_q^{lower} is around 5 cm when $\delta r_{sep} \leq 0$, while λ_q^{upper} is around 7 cm when $\delta r_{sep} \geq 0$. A similar study has been done on DIII-D [29] although the observed behaviour appears to be opposite to that described here. Simultaneously to the IR measurements, the decay length of the ion saturation current was measured at the machine mid-plane by a reciprocating probe equipped with a Gundestrop-type probe head. Figure 7b shows the results obtained for 6 different pins, which are mapped on the machine midplane. As expected, the derived decay length depends on the actual pin, although the reason for the very large scatter in the data obtained for a magnetically balanced case is not yet understood. In any case, the evolution of the I_{sat} decay length with δr_{sep} is in good agreement with the results described in figure 7a. It thus appears that the observed change in the heat flux profile width is correlated to changes in the SOL width at the mid-plane and is not a consequence of different flux expansions for lower and upper single-null discharges. The total power to the outer target, for otherwise identical discharges, is lower for the case δr_{sep}=4 cm than for the case δr_{sep}=-4 cm, as is the electron temperature. The observed results are thus in line with the observed decrease of the heat flux profile width with increasing power to the target [8].

The heat flux profile width at the secondary divertor also varies with δr_{sep}, and typically increases with δr_{sep} as illustrated in 7a. The large scatter in the data is probably linked to the low IR signal measured at the secondary strike point. Following the installation of the LWIR camera, filamentary structures have been regularly at the outer divertor during L-mode discharges as shown in 8. These L-mode filaments are regularly observed by fast-visible cameras in MAST and a detailed study of their nature is reported in [30]. The temporal evolution of the heat flux profile during a L-mode

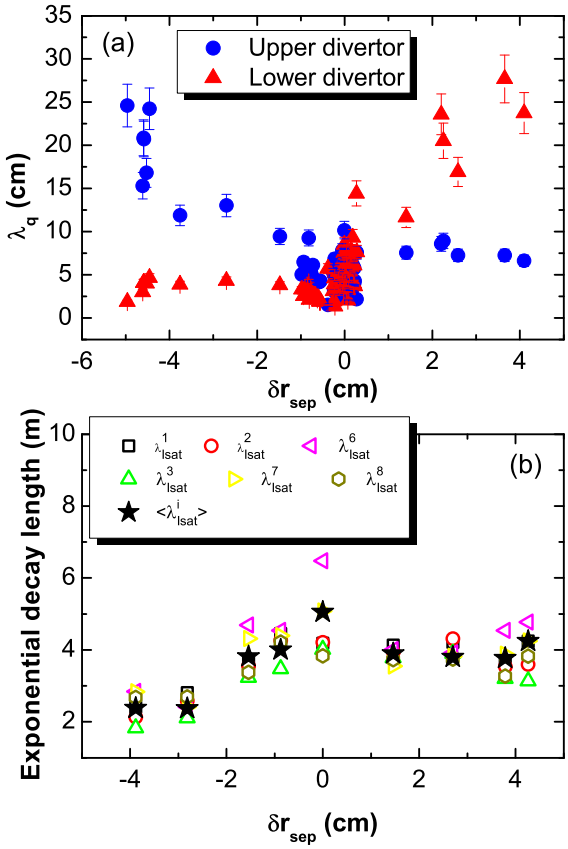

Figure 7. (a) Heat flux profile width (λ_q) on the outer divertor and (b) exponential decay length of the ion saturation current (mapped to the midplane) measured with the midplane reciprocating probe as a function of the distance between the 2 separatrices.

discharge is shown in fig. 9. In this case the camera was working with a framerate of 3.4 kHz. The filamentary structure of the heat flux profile can be clearly seen although the energy deposited far from the strike-point is very low. Heat deposition from such filaments can still be seen 15 cm away from the strike-point. Those results are consistent with earlier observations from ASDEX-Upgrade [28] where the heat flux profile had 2 characteristic widths. The second width in our case appears to be linked with power deposition by filaments which diffused radially outwards. In SND discharges, the heat flux profile width will mainly be defined by this mechanism as the filaments have to intercept the second separatrix in order to be transported to the secondary strike point.

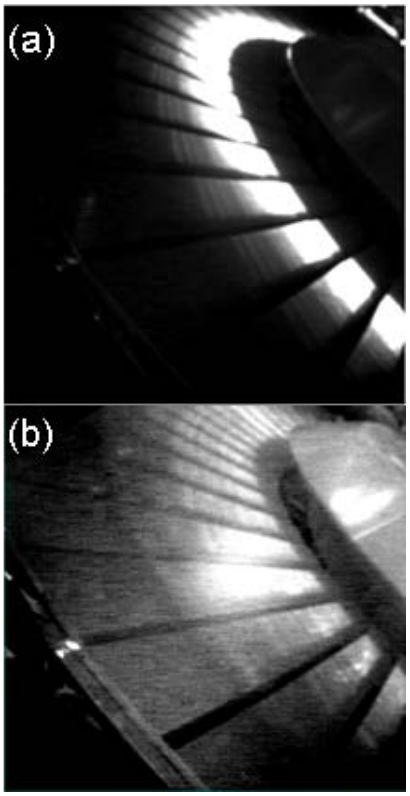

Figure 8. Infrared images of the upper outer divertor target showing filamentary structures during (a) DND and (b) SND L-mode discharges. The brightness and contrast of the pictures has been modified for ease of visualization.

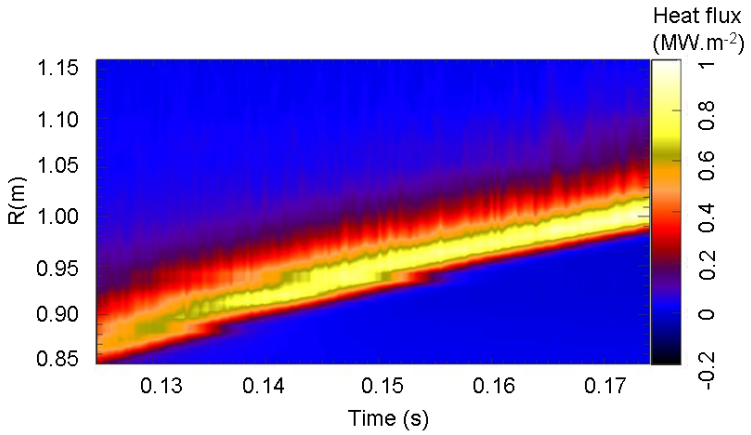

Figure 9. Temporal evolution of the heat flux profile at the upper outer divertor during a L-mode discharge.

5. Conclusions

The installation of a second infrared camera working in the long wave IR has allowed a careful study of heat load asymmetries during L-mode discharges. Temperature

measurements in the LWIR range are found to be less disturbed by surface effects than MWIR measurements. Indeed surface temperatures derived from LWIR measurements are systematically lower than those determined in the MWIR, making LWIR measurements very valuable for tokamaks with cold graphite walls. In MAST, it has been observed that the surface effect disturbance to temperature measurements is different for the inner and outer divertor as well as for the upper and lower divertors. While dust or hot spots appear to be the predominant effect for the outer lower divertor, it is assumed that the upper divertor is mainly affected by co-deposited layers. The next step will be to use combined LWIR/MWIR imaging to derive the bulk tile temperature.

The power repartition between the 4 strike points has been studied as a function of δr_{sep}. In all cases, most of the energy to the SOL goes to the outer divertor(s). The peak in/out asymmetry is obtained for DND discharges. With the $\bigtriangledown B$ drift pointing towards the lower divertor, an asymmetric evolution of the in/out asymmetry with δr_{sep} has been observed with more power going to the outer divertor in upper single-null discharges than during lower single null discharges. The heat flux profile width at the secondary strike point increases with increasing δr_{sep}. Filamentary structures are clearly observed at the outer divertor target and although the time resolution of the IR system is not high enough to capture the full dynamics, power deposition by such filaments is clearly observed far from the strike point.

References

[1] Federici G. *et al* 2001 *Nucl. Fusion* 41 1967

[2] Lasnier C.J. *et al* 1998 *Nucl. Fusion* 38 1225

[3] Chankin A.V. *et al* 1994 *Plasma Phys. Control. Fusion* 36 403

[4] Fuchs J.C. *et al* 1994 *Proc. 21st Eur. Conf. Montpellier, Vol. 18B, Part III* 1308

[5] Nagashima K. *et al* 1995 *J. Nucl. Mater.* 220-222 208

[6] Kirk A. *et al* 2004 *Plasma Phys. Control. Fusion* 46 551

[7] Loarte A. *et al* 2007 *Nucl. Fusion* 47 203

[8] Ahn J-W *et al* 2006 *Plasma Phys. Control. Fusion* 48 1077

[9] Delchambre E. *et al* 2009 *Plasma Phys. Control. Fusion* 51 055012

[10] Reichle R. *et al* 2003 *J. Nucl. Mater.* 313-316 711

[11] Clement S. *et al* 1999 *J. Nucl. Mater.* 266-269 285

[12] Andrew P. *et al* 2005 *J. Nucl. Mater.* 337-339 99

[13] Cox M. 1999 *Fus. Eng. Design* 46 397

[14] Reichle R. *et al* 2001 *J. Nucl. Mater.* 290-293 701

[15] Herrmann A. 2005 *J. Nucl. Mater.* 337-339 907

[16] Reichle R. *et al* 2003 *Nucl. Fusion* 43 797

[17] Herrmann A. *et al* 2004 *Nucl. Fusion* T111 98

[18] Hildebrandt D. *et al* 2005 *J. Nucl. Mater.* 337-339 1064

[19] Tabasso A. *et al* 2002 *J. Nucl. Mater.* 306 73

[20] Ossenkopf V. *et al* 1994 *Astron. Astrophys.* 291 943

[21] Delchambre E. *et al* 2009 *Poster contribution to the 12th PFMC conference,Juelich, Germany, May 2009*

[22] Hermann A. *et al* 2001 Limitations for divertor heat flux calculations of fast events in tokamaks*27th Conf. on Plasma Physics and Controlled Fusion* (contribution)

[23] Herrmann A. *et al* 1995 *Plasma Phys. Control. Fusion* 37 17

[24] Lott F. *et al* 2002 *J. Nucl. Mater.* 337-339 786

[25] Eich T. *et al* 2007 *Plasma Phys. Control. Fusion* 49 573

[26] Arnas C. *et al* 2009 *J. Nucl. Mater.* submitted

[27] Matthews G.F. 2005 *J. Nucl. Mater.* 337-339 1

[28] Pitcher C.S. and Stangeby P.C. 1997 *Plasma Phys. Control. Fusion* 39 779

[29] Petrie T.W. *et al* 2001 *J. Nucl. Mater.* 290-293 935

[30] Dudson B.D. *et al* 2008 *Plasma Phys. Control. Fusion* 50 124012